

Local Energy Gap in Deformed Carbon Nanotubes

K. Sasaki and Y. Kawazoe

Institute for Materials Research, Tohoku University, Sendai 980-8577, Japan

R. Saito

Department of Physics, Tohoku University and CREST, JST, Sendai 980-8578, Japan

(Dated: December 20, 2019)

The effects of graphite surface geometrical deformation on the dynamics of conducting electrons are investigated theoretically. The analysis is performed within the framework of a deformation-induced gauge field and corresponding deformation-induced magnetic field. It is shown that the latter gives a local energy gap along the axis of a deformed nanotube. We compare our energy gap results with experimental data on energy gaps in nanotubes and peapods. We also discuss the mixing of two Fermi points and construct a general model of low energy dynamics including a short-range deformation of the graphite sheet. The derived model is equivalent to the Weyl equation in U(1) Abelian and SU(2) non-Abelian deformation-induced gauge fields.

I. INTRODUCTION

The geometric structure of materials and their electronic or magnetic properties are closely related to each other. It is widely recognized that carbon nanotubes [1] provide us with a great opportunity to study such a relationship. For instance, a single-wall carbon nanotube (SWNT) exhibits either metallic or semiconducting behavior dependent on the lattice structure around the tube axis [2, 3]. When a graphene sheet is folded into a cylinder to form a carbon nanotube, the deformation of the graphite surface changes the dynamics of conducting electrons by modifying the overlap integral of nearest-neighbor orbitals. The energy dispersion relation of the graphite surface is unique because of the linear dispersion relation at the two distinct Fermi points (the K and K' points). In a honeycomb lattice structure, the linear energy dispersion relation leads to the Weyl equation [4]. In this case, the perturbation due to atomic deformation appears in the dynamics through the gauge coupling [5]. A conducting electron moves on the deformed graphite sheet in which the deformation can be expressed by a deformation-induced gauge field. The effect of finite curvature on the low-energy dynamics was clarified by Kane and Mele [5]. They showed that the curvature effect can be included as an effective gauge field shifting the Fermi point in the Brillouin zone by the Aharonov-Bohm effect. Their theoretical result for the energy gap induced by the curvature effect was proved by the scanning tunneling spectroscopy (STS) experiment of Ouyang et al. [6] and was applied to different chiral structures by several authors [7]. In this paper, we generalize the idea of the effective gauge field to a local deformation of the graphite surface and show that the deformation-induced gauge field for locally deformed lattice will provide the local energy gap, which will be useful for describing finite scaled nanomaterials.

In Sec. II and III, we illustrate how the electron dynamics depends on the geometry of a deformed surface. In particular, we consider how a local deformation affects

the local electrical properties of conducting electrons in SWNTs in terms of the deformation-induced gauge field. We point out here that the deformation-induced gauge field and usual electromagnetic gauge field are different from one another, though we can use the analogy in many cases. Furthermore, the deformation-induced magnetic field concerns not the spin of an electron but its pseudo-spin [8] as defined by the two sublattices of graphite and SWNTs. In Sec. IV, we clarify the relationship of the atomic deformation with a local energy gap structure. We compare our theoretical result with the local energy gap observed by STS in nanotubes [6] and peapods [9]. In Sec. V, we consider a short range deformation that results in a mixing of the wave functions at two Fermi points, and we construct an effective model for the low-energy dynamics.

II. DEFINITION OF THE GAUGE FIELD FOR DEFORMATION

The quantum behavior of conducting electrons on a graphite surface is described by the nearest-neighbor tight-binding Hamiltonian as

$$H_{\text{near}} = \sum_{\langle i, j \rangle A} V_a(r_i) a_{i+A}^{\dagger} a_i + h.c.; \quad (1)$$

where A (in the summation index) denotes an A-sublattice, a_i and a_i^{\dagger} are canonical annihilation-creation operators of the electron at site i that satisfy the anti-commutation relation $a_i a_j^{\dagger} = \delta_{ij}$, and site $i + A$ indicates the nearest-neighbor sites ($A = 1, 2, 3$) of site i. We include deformation on the graphite surface as the position-dependent hopping integral $V_a(r_i)$ in the Hamiltonian. We decompose the hopping integral into the two components: $V_a(r_i) = V + V_a(r_i)$, and de ne

$H_{\text{near}} = H_0 + H_{\text{deform}}$ where

$$H_0 = \frac{X}{a} \frac{X}{i2A} V a_{i+a}^y a_i + h.c.; \quad (2)$$

$$H_{\text{deform}} = \frac{X}{a} \frac{X}{i2A} V_a(r_i) a_{i+a}^y a_i + h.c.; \quad (3)$$

Hereafter we refer to the deformed Hamiltonian as H_{deform} . The total Hamiltonian adopted for this study is $H_{\text{near}} = H_0 + H_{\text{deform}}$, which is not easy to solve for general $V_a(r_i)$. However, as far as we consider the physics near the Fermi level, we can obtain several important physical consequences. For example, the model Hamiltonian can exhibit a local energy gap [9] for a specific deformation $V_a(r_i)$.

We follow the effective-mass description [10] for low-energy conducting electrons around the Fermi level. Here, we first consider the case in which the deformation is sufficiently delocalized compared with the diameter of an SWNT such that there is no interaction between two Fermi points. In this case, we will have doubly degenerated electronic states near the K and K' points. The effective Hamiltonian at K-point H_K is given by

$$H_K = v_F (p - A); \quad (4)$$

where we have denoted $p = p_1 + p_2$ and $A = A_1 + A_2$, where A is a vector field defined on the surface, v_F is the Fermi velocity and a_i ($i = 1, 2, 3$) are the Pauli matrices given by

$$a_1 = \begin{pmatrix} 0 & 1 \\ 1 & 0 \end{pmatrix}; \quad a_2 = \begin{pmatrix} 0 & i \\ i & 0 \end{pmatrix}; \quad a_3 = \begin{pmatrix} 1 & 0 \\ 0 & 1 \end{pmatrix}; \quad (5)$$

We adopt the coordinate around (along) the axis as x_1 (x_2). The first term $v_F p$ describes the dispersion of H_0 [4], and the second term $v_F A$ denotes the dispersion of the deformed Hamiltonian. Field $v_F A(r)$ is given by a linear function of $V_a(r)$. We will show an explicit form for $A(r)$ in the next section, but here we note two points. First, the deformation can be included as a gauge field because of the gauge coupling $p \cdot A$. We call A the deformation-induced gauge field and distinguish it from the electromagnetic gauge field A^{em} . Note that A does not break the time-reversal ($T \rightarrow T$) symmetry because the sign in front of A is different for K and K' points, contrasted with the T -violating nature of A^{em} (see Eq. 27). The second point is that we can decompose any gauge field into the sum of a constant, rotation-less, and divergence-less component as

$$A_i = A_i^0 + \theta_{i+a} + \epsilon_{ij} \theta_{j+b}; \quad (i, j = 1, 2); \quad (6)$$

where ϵ_{ij} is the antisymmetric tensor ($\epsilon_{12} = \epsilon_{21} = 1$), and a and b are regular scalar functions defined on the tube surface.

Several important physical properties can be derived from H_K through dimensional reduction. We integrate

H_K over the circumference coordinate (x_1) to obtain a one-dimensional theory as

$$I \frac{dx_1}{C_h} H_K = v_F (p_1^0 - A_1^0 - m(x_2))_1 + v_F (p_2 - A_2^0)_2; \quad (7)$$

where C_h is the circumferential length, p_1^0 is determined by the chiral index, and

$$m(x_2) = \frac{dx_1}{C_h} \theta_2 - b(x_1; x_2); \quad (8)$$

The function θ_2 for A_1 disappears with integration over the x_1 -coordinate. We have neglected the θ_2 part for A_2 because it can be expressed by a phase of the wave function. We identify the p_1 term with the mass of a particle propagating along the axis direction (x_2). This is because (1) the energy spectrum at position x_2 is bounded by the square root of the sum of squares of each coefficient of the Pauli matrices in Eq.(7) as

$$q \sqrt{(p_1^0 - A_1^0 - m(x_2))^2 + (p_2 - A_2^0)^2}; \quad (9)$$

and (2) p_2 scales as inverse of the system length ($l = \pi C_h$) and hence $p_2 - A_2^0$ can be neglected in comparison with $p_1^0 - A_1^0 - m(x_2)$ for a long system ($\pi C_h \gg l$). We define a local energy gap as the minimum energy gap for long tubes, given by

$$E_{\text{gap}}(x_2) = 2v_F \frac{p_1^0 - A_1^0 - m(x_2)}{C_h} = 2v_F \frac{p_1^0}{C_h} \frac{dx_1}{C_h} A_1(x_1; x_2); \quad (10)$$

Since the circumferential component (A_1) of the deformation-induced gauge field is determined by the modulation part of the hopping integral, knowing $V_a(r)$ allows us to calculate the local energy gap using the above formula. The modulation part of the hopping integral can be calculated by choosing a specific scheme. We adopt the Slater-Koster scheme and apply the formula to several deformed nanotubes. In the next section, we present a detailed derivation and a general formula applicable to an arbitrary chiral index.

III. DERIVATION OF THE LOCAL ENERGY GAP

First we show an explicit form of A by $V_a(r_i)$. We rewrite Eq.(2) using the Bloch basis vector as

$$H_0 = V \sum_k f(k) j_A^k i h_B^k j + h.c.; \quad (11)$$

where we have defined $f(k) = \sum_a f_a(k)$ and $f_a(k) = e^{ik \cdot R_a}$. Here, R_a ($a = 1, 2, 3$) are vectors pointing to the nearest-neighbor sites of an A-site (Fig. 1). We have defined the Bloch basis vectors with wave vector k as

$$j^k_i = \frac{1}{N} \sum_{i2}^X e^{ik \cdot R_a} a_{i+a}^y j_i; \quad (12)$$

where the ($= A; B$) indices denote two sublattices as illustrated in Fig. 1, and $N_A (= N_B)$ denotes the number of black (white) sites represented by solid (empty) circles. Here, r_i labels the vector pointing toward each site i , and H_0 consists of momentum preserving interactions ($k \neq k$) only because of the translational symmetries. However, H_{deform} contains the momentum transferring term ($k \neq k + k$).

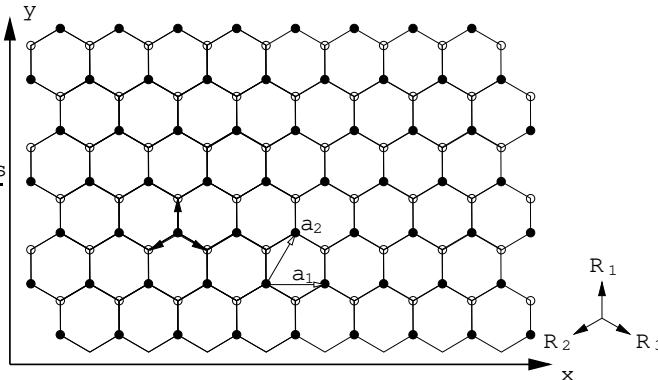


FIG. 1: Structure of a honeycomb lattice having the two symmetry translation vectors $a_1 = \frac{1}{3}a_{cc}e_x$ and $a_2 = (\sqrt{3}=2)a_{cc}e_x + (3=2)a_{cc}e_y$, where e_x and e_y are unit vectors, and a_{cc} is the nearest-neighbor bond length. The black (white) circles indicate the A (B) sublattices. Vectors R_a ($a = 1, 2, 3$) point to the nearest-neighbor sites of an A-site. They are given by $R_1 = a_{cc}e_y$, $R_2 = (\sqrt{3}=2)a_{cc}e_x - (1=2)a_{cc}e_y$ and $R_3 = (\sqrt{3}=2)a_{cc}e_x + (1=2)a_{cc}e_y$.

We expand Eq.(11) around the K -point k_F as

$$H_0 = V \sum_a f_a(k_F) i(k - k_F) R_j \frac{k}{a} i h \frac{k}{B} j +$$

where we have used a condition of Fermi point $f(k_F) = 0$ (we can set $f_1(k_F) = 1$, $f_2(k_F) = e^{i\frac{2\pi}{3}}$ and $f_3(k_F) = e^{+i\frac{2\pi}{3}}$). The lattice structure of SWNTs is specified by the chiral and translational vectors defined by $C_h = n a_1 + m a_2$ and $T = p a_1 + q a_2$, where a_1 and a_2 are symmetry translation vectors on the planar honeycomb lattice (Fig. 1). The corresponding wave vector k can be decomposed as $k = k_1 + k_2$, where k_1 and k_2 are integer coefficients of vectors k_1 and k_2 that satisfy $C_h \cdot k = 2$, $C_h \cdot k = 0$, $T \cdot k = 0$ and $T \cdot k = 2$. With these definitions, the first term on the right-hand side of Eq.(13) is rewritten as

$$V e^{i w} j \frac{k}{A} i h \frac{k}{B} j \quad (14)$$

where $w = w_1 - i w_2$, w_1 and w_2 are given by

$$w_1 = \frac{3a_{cc}}{2\mathcal{C}_h j} (2 - 1 - k_F - T); \quad (15)$$

$$w_2 = \frac{3a_{cc}}{2\mathcal{C}_h j} (2 - 2 - k_F - T); \quad (16)$$

and angle satisfies

$$n + \frac{m}{2} \frac{p - \frac{3}{2}m}{2} = \frac{p - \mathcal{C}_h j}{3a_{cc}} e^{i \theta}; \quad (17)$$

To obtain Eq.(14), it is useful to rewrite R_a in terms of the chiral and translational vectors as

$$\begin{aligned} R_1 &= \frac{2}{3N_c} h p + \frac{q}{2} C_h n + \frac{m}{2} T^i; \\ R_2 &= \frac{2}{3N_c} h p - \frac{q}{2} C_h + \frac{n - m}{2} T^i; \\ R_3 &= \frac{2}{3N_c} h p + q C_h + \frac{n + m}{2} T^i; \end{aligned} \quad (18)$$

where we have introduced $N_c = m p - n q$ and used the relationship $(3\sqrt{3}=2)a_{cc}^2 N_c (e_x - e_y) = T - C_h$. Finally, leading term of the Hamiltonian matrix for H_0 can be expressed in the basis of the two sublattices ($A; B$)^t by

$$H_0 = V \begin{pmatrix} 0 & e^{i w} \\ e^{-i w} & 0 \end{pmatrix}; \quad (19)$$

Next, we consider the momentum transfer matrix element of H_{deform} :

$$h \frac{k+}{A} \frac{k}{B} j \frac{k}{B} i = \frac{1}{N_A} \sum_{i \in A} \sum_{a} V_a(r_i) f_a(k) e^{i k \cdot r_i}; \quad (20)$$

where we have used Eqs.(3) and (12) to get the right-hand side. Here, we restrict ourselves to considering the momentum transfer matrix element that does not mix the two Fermi points ($j \neq k \neq k_F$). We then set $k = k_F + k^0$ and obtain

$$h \frac{k+}{A} \frac{k}{B} j \frac{k}{B} i = \frac{1}{N_A} \sum_{i \in A} \sum_{a} V_a(r_i) f_a(k_F) e^{i k \cdot r_i}; \quad (21)$$

where we omit a correction on the order of $O(V_a k^0)$. The momentum k and $k + k^0$ in the last equation should be recognized as being restricted to the wave vector around the K point. Up to the leading order, this shows that the electrons near the K -point feel the "local potential" given by $V_a(r_i) f_a(k_F)$ because its Fourier component appears in the right-hand side of Eq.(21). It is valuable to note that there is a similarity between the deformation Hamiltonian and a potential $V(x)$ (whose constant component should be subtracted) for a particle of mass m . Let us consider a simple one-dimensional Hamiltonian,

$$H = \frac{p^2}{2m} + V; \quad (22)$$

When we consider the matrix element of the potential term between free particle states denoted as $|ki\rangle$ with a definite momentum, we obtain

$$\hbar k + k_F \langle j | = \frac{dx}{L} V(x) e^{ikx}; \quad (23)$$

where L is the system length. This should be compared with Eq.(21) and shows that $\langle a | V_a(r_i) f_a(k_F) | \rangle$ works as a potential. Note also that Eq.(19) corresponds to the kinetic term of Eq.(11).

Combining Eq.(19) with Eq.(21), we get the effective mass Hamiltonian

$$\begin{aligned} V &= \begin{pmatrix} 0 & e^{i\omega} & & \\ e^{i\omega} & 0 & & \\ & & \Psi & A \\ & & & \end{pmatrix} \\ &= \begin{pmatrix} e^{i\omega} & 0 & & \\ 0 & e^{i\omega} & V_F & \\ & & p & e^{i\omega} \\ & & & 0 & e^{i\omega} \end{pmatrix} \quad A; \quad (24) \end{aligned}$$

where we have denoted $\langle a | V_a(r_i) f_a(k_F) | \rangle$ as $\Psi(A_x, iA_y)$ and used $f_1(k_F) = 1$, $f_2(k_F) = e^{i\frac{2\pi}{3}}$ and $f_3(k_F) = e^{i\frac{4\pi}{3}}$. Here, we have defined the Fermi velocity as $V_F = 3V_{acc}/2h$, $p = (2h/3a_c)(_1w_1 + _2w_2)$, and $A = _1A_x + _2A_y$. Then, functions (A_x, A_y) are given by

$$\Psi A_x = V_1 - \frac{1}{2} V_2 - \frac{1}{2} V_3; \quad \Psi A_y = \frac{p}{3} (V_2 - V_3); \quad (25)$$

This is the explicit relationship between the hopping modulation and the deformation-induced gauge field. We refer to functions (A_x, A_y) , or the appropriate linear combination, as the deformation-induced gauge field. This is because the effects of the deformation can be included in the theory through the substitution $p \rightarrow p + A$. This is the same substitution as for an electromagnetic gauge field. It is useful for understanding the emergence of gauge interaction to consider electrons near the Fermi level in one-dimensional system defined in Eq.(22). We obtain the following effective dynamics around the Fermi momentum p_F :

$$H = \frac{p_F}{m} p + V(x) = V_F p + \frac{V(x)}{V_F}; \quad (26)$$

which also indicates that the potential term behaves as a gauge field. Here, we set $p \rightarrow p_F + p$ in Eq.(22) and the Fermi velocity as $V_F = p_F/m$.

Here, we simplify the notation in Eq.(24) and remark on a general property of the effective Hamiltonian. We have two distinct modes, the dynamics of which are approximated by the following two effective Hamiltonians in the presence of external electromagnetic gauge field A^em as

$$H_K = V_F (p + A - \frac{1}{2} A^em); \quad H_{K^0} = V_F (p + A + \frac{1}{2} A^em); \quad (27)$$

where we have defined $= (1; 2)$ and $= (1; 2)$. H_{K^0} can be obtained by expanding Eq.(11) around the K' -point k_F and repeating the calculation presented

above. Our notation of the momentum is $p = _1p_1 + _2p_2$ ($^0 p = _1p_1 + _2p_2$) where

$$p_1 = \frac{h(2 - 1 - k_F - \zeta)}{C_h j}; \quad p_2 = \frac{h(2 - 2 - k_F - T)}{J j}; \quad (28)$$

and our notation of the deformation-induced gauge field is $A = _1A_1 + _2A_2$ ($^0 A = _1A_1 + _2A_2$) where

$$\begin{aligned} A_1 &= \cos \frac{\sin}{\sin} \frac{A_x}{A_y} : \\ A_2 &= \sin \frac{\cos}{\cos} \frac{A_x}{A_y} \end{aligned} \quad (29)$$

Note that p_1 (p_2) is the momentum around (along) the axis measured from the K' point. As for the K' point, k_F and ζ should change their sign, and correspondingly p_1 for the K' point will have a sign opposite to that of the K point. Notice also the different sign for A of the K and K' points, in contrast to the same sign for A^em in Eq.(27). Therefore, in the absence of an external electromagnetic gauge field, time-reversal symmetry is preserved even in the presence of deformation.

By virtue of the decomposition of Eq.(6) with the gauge coupling structure of Eq.(27), the following two points become clear. The first is that the ζ component does not change the energy spectra of the theory because it can be eliminated by multiplying the phase of the wave function ($\zeta e^{i\frac{\zeta}{h}}$). However, it should be mentioned that a nontrivial functional form of ζ gives a nonvanishing divergence of the deformation-induced gauge field, represented by $\zeta A = \frac{1}{2} \zeta \not{A} \neq 0$. This may correspond to the deformation potential and could cause a local (background) charge modulation [11]. A negative one-dimensional quantum field theory derived from Eq.(27) can be classified as the Tomonaga-liquid theory [12], and can be used in that framework to study this effect. The analysis shows that it does not change the energy spectrum of the theory but gives only a charge density modulation for metallic cases. The second point is that function b operates as a source of a deformation-induced magnetic field and can lead to an important physical effect. The curl part of the deformation-induced gauge field defines a deformation-induced magnetic field as

$$B_? = \epsilon_{ij} \not{A}_i A_j = r^2 B; \quad (30)$$

whose direction is perpendicular to the graphite surface, and a nontrivial magnetic field gives a local modulation of the energy gap as defined in Eqs.(8) and (10).

We integrate in Eq.(7) over the circumferential coordinate (x_1) of Eq.(27). In Eq.(7), p_1^0 is determined by setting $\zeta = 0$ in Eq.(28), and ζ relates to the chiral index via $\zeta = h(2n+m)/3$ (where hxi indicates the closest integer to the number x , that is, rounded x). Note that we have already neglected the term

$$\epsilon_2 \int_1^I \frac{dx_1}{C_h j} a(x_1; x_2) \quad (31)$$

in Eq.(7) by selecting a proper phase for the wave function. The coefficient of ζ works as the effective mass of

a particle propagating along the axis. Then, $p_1^0 A_1^0$ is related to a position-independent mass and $m(x_2)$ expresses a local modulation of the mass. They combine to give the local energy gap of Eq.(10).

It is valuable to note that the position-dependent mass (or local energy gap) corresponds to the existence of the local deformation-induced magnetic field because if a nonvanishing local energy gap remains then its first derivative about the axis direction (x_2) also gives a non-vanishing value. This corresponds to the magnetic field integrated about coordinate x_1 as

$$\oint_2 m(x_2) = \frac{dx_1}{\mathcal{C}_h j} \oint_2 \theta_2^2 b = \frac{dx_1}{\mathcal{C}_h j} B_2(x_1; x_2); \quad (32)$$

The Stokes theorem allows us to imagine a deformation-induced magnetic field B_k in the cylinder, defined by the loop integration of the deformation-induced gauge field around the axis, given by

$$\oint B_k(x_2) S = \int dx_1 A_1(x_1; x_2); \quad (33)$$

where S denotes the cross-sectional area of the cylinder assumed to be constant along the axis. When the magnetic field escapes from within the cylinder, it penetrates the surface. This corresponds to B_2 on the surface (penetrating the surface) and then changes the mass of the particle (see Fig. 2).

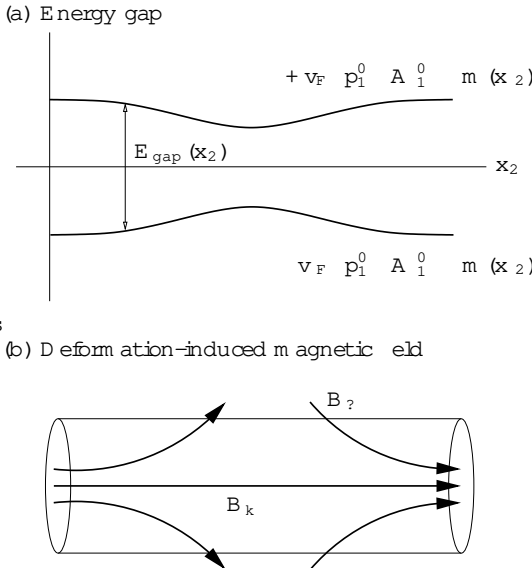


FIG. 2: The relationship between (a) the local energy gap and (b) the corresponding deformation-induced magnetic field B_k and B_2 . It is noted that this is not the usual electro-magnetic field.

Let us refer to an interesting case where $p_1^0 A_1^0 m(x_2)$ changes its sign at some position. It is known that an unusual solution, the Jackiw-Rebbi modes [13] (electron-deformation bound states), exists at the band center. Such a condition will likely be fulfilled for the bulk part of some types of peapod carbon nanotubes.

IV. EXAMPLES OF DEFORMATION-IN DUCED GAUGE FIELDS

In this section, we apply the theory in a curved surface of SWNT. First we classify two types of deformation by the Slater-Koster scheme defined as

$$V_a(r_i) = V(a_{cc} + r_a)e(r_{i+a}) e(\mathbf{f}); \quad (34)$$

which can include the fact that conducting electrons make a σ -orbital whose wave function extends in the normal direction $e(r_i)$ of the surface. Here, $V(r)$ is a function of the bond length r ($V(a_{cc}) = V$) and $e(r_i)$ is a unit normal vector at r_i . We have assumed here that the effect of the bond is included in the definition of $V(r)$.

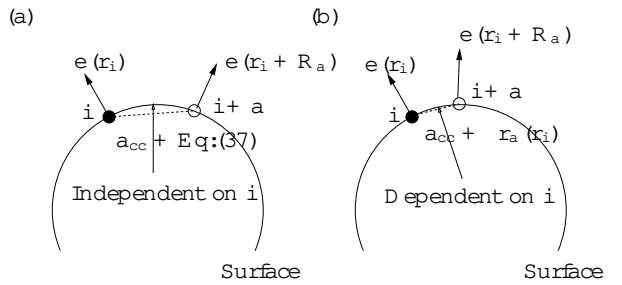


FIG. 3: A schematic diagram of the deformed surface of a two-dimensional graphite sheet. In these diagrams, only two sites (i and $i+a$) are depicted. We denote the direct distance between them by $a_{cc} + r_a$. We classify (a) as the bond-bending type and (b) as the bond-stretching type in this paper. In (a), the direct distance is given by $a_{cc} + \text{Eq.(37)}$, and in (b) it is not related to the normal vector.

Now, $e(r_i + R_a)$ can be expanded in Taylor series around $e(r_i)$ as

$$e(r_i + R_a) = e(r_i) + (R_a - r)e(\mathbf{f}) + \frac{1}{2}(R_a - r)(R_a - r)e(\mathbf{f}) + \dots \quad (35)$$

Using the normalization condition of the normal vector $e(r_i) \cdot e(\mathbf{f}) = 1$, we obtain $e(r_i) \cdot (R_a - r)e(\mathbf{f}) = 0$. We can then write $V_a(r_i) = V_a(r_i) + V$ as

$$V_a(r_i) = r_a(r_i)(\partial V / \partial a_{cc}) + V \frac{1}{2}e(r_i)(R_a - r)(R_a - r)e(\mathbf{f}) + \dots \quad (36)$$

where \dots denotes higher order corrections. As for nanotubes, the derivative $(\partial V / \partial a_{cc})$ is scaled by the inverse of the circumferential length ($\mathcal{C}_h j$) or by the inverse of the total length ($\mathcal{J} j$), depending on the direction. We can therefore consider, as the order estimation, that the relevant energy of the second term on the right-hand side of Eq.(36) is proportional to an inverse square of circumferential length $V a_{cc}^2 = \mathcal{C}_h j^2$. This gives a small (but observable [6]) correction to the energy gap. On the other

hand, the bond length modulation denoted by $r_a(r_i)$ may give a dominant contribution to the energy gap [9]. Hereafter, we shall define two types of deformation depending on the functional form of $r_a(r_i)$.

The first type of geometry includes the deformed surfaces of SWNTs. The bond length modulation between adjacent carbon atoms for this geometry, as shown in Fig. 3(a), is defined by

$$r_a = \frac{a_{cc}}{12} \frac{1}{2} e(r_i) (R_a - r) (R - r) e^{\frac{r}{R}} + \dots \quad (37)$$

By substituting this into Eq.(36), we obtain

$$V_a(r_i) = D (R_a - r) e^{\frac{r}{R}} (R - r) e^{\frac{r}{R}} \quad (38)$$

where we have introduced the constant

$$D = \frac{1}{2} \frac{1}{12} a_{cc} \theta V j_{cc} + V \quad (39)$$

for the sake of convenience. Incidentally, the numerical value of D can be estimated from the experimental data of Ouyang et al. [6] as $\theta j = V = 8$, with $V = 2.60$ [eV]. We classify deformed surfaces whose hopping integral is approximated by Eq.(38) with an appropriate D into the bond-bending deformation type. The hopping integral of the bond-bending type is calculated from the normal vectors on the surface, which means that we only need to parameterize the surface and do not need to perform microscopic calculations to obtain the hopping integral. Notice we assume here that the (indirect) distance between two adjacent atoms defined by the line integral of the differential line element on a deformed graphite surface, is fixed by a_{cc} and is independent of its position. This defines the type of geometry having a curved surface.

In another type of deformation, the dominant contribution to $V_a(r_i)$ comes from a change in the bond length. For this type, the hopping integral is well approximated by the first term on the right-hand side of Eq.(36) as

$$V_a(r_i) = (\theta V j_{cc}) r_a(r_i) + \dots \quad (40)$$

Equation (40) may become relevant to the conducting electrons in a peapod-like structure [9], where elastic strain is expected to modify the bond length. We classify deformed surfaces whose hopping integral is approximated by Eq.(40) as the bond-stretching deformation type. The bond length (and its hopping integral) can be calculated by a first-principle calculation.

Table I shows the deformation types. A typical energy of $D a_{cc}^2 = \theta C_h j^2$ is expected for a deformed Hamiltonian of the bond-bending type, and an energy of $(a_{cc} \theta V j_{cc}) r_a = a_{cc}$ for the bond-stretching type.

A. Application to Several Geometries

In this subsection, we present examples of the deformation-induced gauge field with calculated results

Type	$V_a(r_i)$ Target	Energy scale
Bond-bending	Eq.(38) Nanotubes	$D a_{cc}^2 = \theta C_h j^2$
Bond-stretching	Eq.(40) Peapod, etc. $(a_{cc} \theta V j_{cc}) r_a = a_{cc}$	

TABLE I: Deformation types and expected energy scales. The bond-bending type can be applied to ordinary single-wall nanotubes, and the bond-stretching type is expected to be effective for peapod nanotubes.

(37)

for the local energy gap. We calculate the deformation-induced gauge field for several geometries, nanotube and peapod, each of which is classified as a bond-bending or bond-stretching deformation. We then apply the deformation to the local energy gap formula and compare the results with experimental data. We also briefly discuss the effects of the external electromagnetic gauge field and on-site energy.

1. Narrow energy gap in a metallic zigzag nanotube (bond-bending type)

For geometries with a bond-bending deformation, we can apply Eq.(38) to the deformation-induced gauge field. In this case, by substituting Eq.(18) into Eq.(38), and using Eq.(25), we obtain

$$v_F A_x = F_x^{uu} e_u - e + F_x^{uv} e_u - e + F_x^{vv} e_v - e \quad (41)$$

$$v_F A_y = F_y^{uu} e_u - e + F_y^{uv} e_u - e + F_y^{vv} e_v - e \quad (42)$$

where we have introduced the following notations:

$$\begin{aligned} F_x^{uu} &= F (p^2 + pq - \frac{1}{2} q^2); \\ F_x^{uv} &= -F (2pn + qn + pm - qm); \\ F_x^{vv} &= F (n^2 + nm - \frac{1}{2} m^2); \\ F_y^{uu} &= -F \frac{p}{3q} (p + \frac{1}{2} q); \\ F_y^{uv} &= F \frac{p}{3} (qn + pm + qm); \\ F_y^{vv} &= -F \frac{p}{3m} (n + \frac{1}{2} m); \end{aligned} \quad (43)$$

In the above equations, we define $F = 4^{-2} D = 3N_c^2$ and dimensionless coordinate $(u;v)$ as $C_h r = \theta C_h = 2 \theta_u$; $T r = \theta j = 2 \theta_v$, and we denote $e_u = \theta_u e$ and $e_v = \theta_v e$. The most dominant contributions to the deformation-induced gauge field are contributed by the F_x^{uu} and F_y^{uu} terms. This is because F itself scales as an inverse square of the nanotube surface area, $(p; q)$ scale as θj and $(n; m)$ scale as $\theta C_h j$. Therefore, each component scales as

$$F_i^{uu} : F_i^{uv} : F_i^{vv} = \frac{a_{cc}^2}{\theta C_h j^2} : \frac{a_{cc}^2}{\theta C_h \theta j} : \frac{a_{cc}^2}{\theta j^2}; \quad i = x, y \quad (44)$$

This scaling indicates that we can neglect the F_i^{uv} and F_i^{vv} terms if $\mathbf{j} \cdot \mathbf{j} = \mathbf{j} \cdot \mathbf{j}$.

Since the chiral and translational indices determine each component listed in Eq.(43), specifying normalized vector e on a specific surface fixes the deformation-induced gauge field completely. We can specify the surface of a tube with a constant radius by the vector $p(u;v) = (\mathbf{j}_h/2 \cos u; \mathbf{j}_h/2 \sin u; v)$. The unit normalized vector of this surface is calculated as $e = (\cos u; \sin u; 0)$. We then obtain $e_u \cdot e = 1; e_u \cdot e = 0; e_v \cdot e = 0$ yielding the deformation-induced gauge field

$$v_F A_x = F_x^{uu}; \quad v_F A_y = F_y^{uu}; \quad (45)$$

To calculate each component of Eq.(43) explicitly, we use the example of zigzag nanotubes, the chiral index of which is $(n;0)$, with metallic index $p_1^0 = 0$ (where n is a multiple of 3). In this case Eq.(43) gives

$$F_x^{uu} = -\frac{2D}{n^2}; \quad F_y^{uu} = 0; \quad (46)$$

Applying this result to the formula for the energy gap of a metallic zigzag nanotube, we obtain $E_{\text{gap}}(v) = 2F_x^{uu}j$. We then compare this with the experimental result of Ouyang et al. [6]. The experiment shows that an energy gap for metallic zigzag SWNTs with $n = 9, 12, 15$ can be fitted by

$$E_{\text{gap}}^{\text{exp}} = \frac{2V}{4n^2} \quad (V = 2.60 \text{ eV}); \quad (47)$$

which corresponds to the parameter $D = V = 8$. Using the explicit form of parameter D , we can read off the first derivative of $V(r)$ as

$$a_{cc} @ V \frac{dV}{dr} = \begin{cases} 9V & \text{if } D < 0 \\ 15V & \text{if } D > 0; \end{cases} \quad (48)$$

which can be used to analyze the other chiral structures and also for geometries of the bond-stretching deformation. It is noted that these values can be compared with the value estimated by another scheme [14, 15] giving $(a_{cc} @ V \frac{dV}{dr}) = 3V$. The reason of this discrepancy is out of scope of our low energy theory, however overall factor of $E_{\text{gap}}^{\text{exp}}$ may be affected by the detail of STS experiments. The important point is that the n -dependence of the energy gap, which is the same for the experiment (although only three different n values are available) and theory. Another possible reason of this discrepancy is that actual nanotubes are in between bond-bending and bond-stretching classes. We can introduce a phenomenological parameter D for describing such a nanotube to Eq.(39) as

$$D = \frac{1}{2} \frac{h}{12} a_{cc} @ V \frac{dV}{dr} + V; \quad (49)$$

We can set $D = 3$ to get $(a_{cc} @ V \frac{dV}{dr}) = 3V$.

2. Peapod (bond-stretching type)

We consider the peapod geometry as an example of a bond-stretching deformation whose hopping integral strongly depends on the bond length modulation. As with some (encapsulated metal fullerene) peapod-like structures [9], elastic strain is expected to modify the bond length. We do not attempt to calculate the bond length for such systems using a first-principle calculation, but instead want to estimate the bond length modulation (necessary for explaining an observed local energy gap modulation within our theoretical framework).

We consider zigzag nanotubes $(n;0)$ with constant radius and assume that $A_1 = A_x$ depends only on the axis coordinate. In this case, we can simplify the formula for the energy gap as

$$E_{\text{gap}}(y) = 2v_F p_x^0 A_x(y); \quad (50)$$

From Eqs.(25) and (40), the deformation-induced gauge field around the axis can be written as

$$v_F A_x(y) = (@V \frac{dV}{dr}) r_1(y) - \frac{1}{2} r_2(y) - \frac{1}{2} r_3(y); \quad (51)$$

It is reasonable to suppose that the bonds, pointing in three different directions, are related to each other because the modulation generates a force between the adjacent atoms. For zigzag, we assume the relation $r_2(y) = r_3(y) = \frac{1}{2} r_1(y)$, which gives an equilibrium configuration and preserves the rotational symmetry around the axis. In this case, the energy gap formula becomes

$$E_{\text{gap}}(y) = 2v_F p_x^0 \frac{1}{2} (a_{cc} @ V \frac{dV}{dr}) \frac{r_1(y)}{a_{cc}}; \quad (52)$$

where the first term on the right-hand side can be given for zigzag nanotubes with chiral index $(n;0)$ as

$$v_F p_x^0 = V \frac{2}{n} \frac{p}{3} \frac{2n}{3} \frac{2n}{3}; \quad (53)$$

To achieve an observed energy gap modulation on the order of 0.4 eV [9], the maximum bond-length modulation should be on the order of $r_1^{\text{max}} = a_{cc} = 50$, where we have used the upper case in Eq.(48). Although this quantity was fixed by the experimental data of Ouyang et al [6], it can be estimated by another scheme [14] as $(a_{cc} @ V \frac{dV}{dr}) = 3V$, in which case the maximum bond length modulation should be about $a_{cc} = 20$. In any case, the small bond length modulation gives a rather strong contribution to the local energy gap. Here, we should note that Cho et al. [16] explained the local energy gap observed by Lee et al. [9] in terms of the gap between NT state and the empty metallofullerene state in the gap of the nanotube.

3. Coexistence of deformation-induced and electro magnetic gauge field

It is valuable to note that the deformation-induced gauge field can give a much larger energy scale compared to the usual (magnetic) gauge field. To show this, we consider the relationship between the deformation-induced gauge field and an external magnetic field applied perpendicularly to the axis. Such an external magnetic field can be derived from an external gauge field by

$$A_1^{\text{em}} = 0; A_2^{\text{em}} = \frac{eB^{\text{em}} \mathcal{J}_h j}{2} \sin u; \quad (54)$$

For a practical range of the external magnetic field (10 Tesla), the deformation-induced gauge field can give a much larger energy scale than that of the external gauge field as

$$v_F \frac{eB^{\text{em}} \mathcal{J}_h j}{2} \quad V \quad 10^9 \frac{\mathcal{J}_h j}{a_{\text{cc}}} B^{\text{em}} = \text{Gauss}; \quad (55)$$

Therefore, for typical SWNTs of $\mathcal{J}_h j = 10a_{\text{cc}}$, the effect of the external magnetic field on the energy gap can be safely ignored even for a magnetic field on the order of 10 Tesla. Note also that when we consider the one-dimensional model, it can be shown that the external field does not change the energy gap because $\text{d}u A_1^{\text{em}} = 0$ and $\text{d}u A_2^{\text{em}} = 0$, in contrast to the deformation-induced gauge field.

4. On-site energy (asymmetry between two sublattices)

Let us briefly comment about on-site interaction. The on-site energy is defined by

$$H_{\text{site}} = \sum_i (r_i) a_i^{\dagger} a_i; \quad (56)$$

where (r_i) denotes the on-site energy. The constant component of the on-site energy determines the origin of the energy and is inactive for the dynamics. On the other hand, its modulation part can exert physical effects on the conducting electrons. The modulation can be divided into a symmetric part and an asymmetric part for two sublattices. They appear in the low-energy Hamiltonian as components of $\mathbb{0}$ (identity matrix) and $\mathbb{3}$ [17], respectively, as

$$H_K = v_F (\mathbb{p} - A) + G(r_b) + P(r) \mathbb{3}; \quad (57)$$

The former $G(r)$ operates as the local electrical potential and the latter $P(r)$ gives the asymmetric potential between the two sublattices. While $G(r)$ does not change the energy gap of the theory, $P(r)$ does. The local energy gap along the axis can be calculated by dimensional reduction as

$$E_{\text{gap}}(k_x) = 2 \sqrt{v_F^2 p_1^0 + \frac{dx_1}{\mathcal{J}_h j} A_1^{\text{em}}} + \frac{dx_1}{\mathcal{J}_h j} P^{\text{em}}; \quad (58)$$

We note that deformation-induced gauge field can increase or decrease the energy gap depending on the sign of A_1 , however the asymmetric potential always increases the energy gap.

V. MIXING OF FERMIPONTS

Until now we have disregarded the matrix element that causes a mixing of the two Fermi points K and K' , the effect of which is on the order of $V_a (2k_F)$. In this section, we set the Fermi velocity to unity, or $v_F = 1$. We begin by introducing the Schrödinger equation, the Hamiltonian of which is given by

$$i\hbar \frac{\partial}{\partial t} \begin{matrix} & K \\ & K' \end{matrix} = \begin{matrix} H_K & 0 \\ 0 & (H_{K'})^0 \end{matrix} \begin{matrix} & K \\ & K' \end{matrix}; \quad (59)$$

where we have defined $(H_{K'})^0$ as $H_{K'}$ (see Eq. 27) with the replacement $(p_1, p_2) \rightarrow (-p_1, p_2)$. Thus, each diagonal block is given respectively by

$$H_K = \begin{matrix} 1 & p_1 & A_1 & A_1^{\text{em}} \\ 2 & p_2 & A_2 & A_2^{\text{em}} \end{matrix};$$

$$(H_{K'})^0 = \begin{matrix} 1 & p_1 & A_1 + A_1^{\text{em}} \\ 2 & p_2 + A_2 & A_2^{\text{em}} \end{matrix};$$

Roughly speaking, p_1 measures the difference between the momenta (around the axis) for the K and K' states (Fig. 4). The $\mathbb{1}$ terms serve as mass terms (or energy gap) when we consider an effective one-dimensional model. In this respect, we note the different signs for an external magnetic field A_1^{em} . Since A_1^{em} can be tuned by a magnetic field along the axis, it can cause an asymmetry in the mass of two modes [18], that is, it can break the T -symmetry.

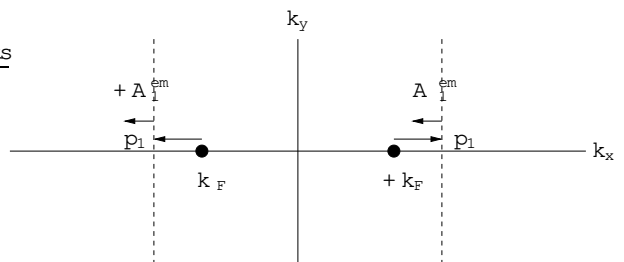


FIG. 4: Momentum representation used in Sec. V. We consider zigzag nanotubes whose Fermi points denoted as solid circles are located on k_x axis. The dashed lines represent two energy bands near the K and K' point.

The matrix defined above is acting on the four component wave function as

$$i\hbar \frac{\partial}{\partial t} \begin{matrix} & K \\ & K' \end{matrix} = \begin{matrix} 0 & 1 \\ B & A \\ B & C \\ B & C \\ K & A \\ K & A \\ K & C \\ K & B \end{matrix} = ; \quad (60)$$

where the two components $_{\text{K}} (_{\text{K}^0})$ correspond to the wave functions at the two sublattices, A and B. The $_{\text{A}}^{\text{K}}$ component couples to the wave functions on the B- sublattice $_{\text{B}}^{\text{K}}$ and $_{\text{B}}^{\text{K}^0}$, and the coupling between $_{\text{A}}^{\text{K}}$ and $_{\text{B}}^{\text{K}^0}$ expresses the mixing effect. Therefore, the general dynamics (except for the topological defects mentioned below) can be described by the Hamiltonian

$$H_e = \begin{pmatrix} 0 & & & & 1 \\ & 0 & (H_K)_{12} & 0 & 2b_1 \\ & B & (H_K)_{21} & 0 & 2b_2 \\ & B & & 0 & 0 \\ & 0 & 2b_2 & 0 & (H_K^0)_{12}^0 \\ 2b_1 & 0 & (H_K^0)_{21}^0 & 0 & \end{pmatrix}; \quad (61)$$

where $b = (b_1; b_2)$ are complex functions.

The mixing of Fermi points may have a strong effect on the dynamics, especially in the presence of pentagons or heptagons in the surface [19]. We try to construct an effective low-energy model including the effects of a topological defect and also the effect of a surface deformation. For that purpose, we first note that the effective dynamics of Eq.(61) can be expressed as a special case of the Schrödinger equation as

$$D = 0; \text{ where } D = (p - A^0)_0 - A^i_i \quad (62)$$

where the summation variable i is understood to take the values $i = (0; 1; 2)$, and D is the covariant momentum. Here, A^i is a generalization of the previously defined deformation-induced gauge field and i is the Pauli matrices (with 0 as the identity element) acting on the wave functions $(_{\text{K}}; _{\text{K}^0})^t$. We have defined $=$ and $p_0 = ih\theta_t$ where t is the time variable. The Schrödinger equation is formally equivalent to the Weyl equation in U(1) Abelian and SU(2) non-Abelian deformation-induced gauge fields.

The Hamiltonian of Eq.(61) can be obtained by setting the generalized gauge field of Eq.(62) as

$$\begin{aligned} A_1^3 &= A_1^{\text{em}}; A_2^0 = A_2^{\text{em}}; \\ A_1^0 &= A_1; A_2^3 = A_2; \\ A_1^1 &= \langle (b_2 + b_1); A_1^2 = (b_1 + b_2); \\ A_2^2 &= \langle (b_1 - b_2); A_2^1 = (b_1 - b_2); \end{aligned} \quad (63)$$

and setting other components to zero. Concerning the relationship between a pentagon or heptagon and the non-Abelian deformation-induced gauge field, the main contribution from a pentagon or a heptagon is the interchange of the wave functions of two Fermi points. This occurs when a low-energy electron moves around the topological defect [19], which can be expressed by a nonvanishing time component of the matrix element $_{\text{1}}$ or $_{\text{2}}$ part as

$$\begin{pmatrix} 0 & ^0(A_0^1 - iA_0^2) & ! & ! \\ & 0 & & \\ ^0(A_0^1 + iA_0^2) & 0 & & \\ & & & _{\text{K}^0} \end{pmatrix} : \quad (64)$$

This is because a pentagon (heptagon) creates a coupling between $_{\text{A}}^{\text{K}}$ and $_{\text{A}}^{\text{K}^0}$ or between $_{\text{B}}^{\text{K}}$ and $_{\text{B}}^{\text{K}^0}$. Hence, the

local dynamics of the low-energy conducting electron on a deformed (graphite) surface is governed by Eq.(62) and the lattice structure fixes the Abelian and non-Abelian deformation-induced gauge field.

V I. DISCUSSION

The main result for the local energy gap (Eq.10) is determined only by the configuration of the deformation-induced gauge field. This is due to the special energy dispersion relation of the graphite sheet which allows us to predict several important physical consequences, not by solving the Hamiltonian explicitly but from the gauge field configuration itself. To understand the configuration of the deformation-induced gauge field, we have classified the geometries into two types: a bond-bending deformation and a bond-stretching deformation. For the bond-bending type, we can extract the gauge field from the geometric information given by the normal vector as we did in Sec. IV A 1, where no microscopic theory is necessary to calculate the field configuration. On the other hand, for the bond-stretching type, we need a microscopic theory capable of predicting the bond length or the gauge field in order to calculate the local energy gap (Sec. IV A 2). We can make a qualitative analysis of the bond-stretching type using a microscopic model and compare it with our local energy gap formula, which will be reported elsewhere.

When we consider the mixing effect due to short range interaction, we should generalize the geometry-induced gauge field from an Abelian to non-Abelian field. Constructing a general low-energy theory is of prime importance because a general deformation may generate a topological defect, such as a pentagon or heptagon, which can mix the wave functions at the two Fermi points. In addition, we can consider a higher genus material, the kinematics of which are nontrivial [20, 21]. One possible way to examine such a material is to extract useful information from a dynamical model.

Finally, we comment on the wave functions in the nanotubes having a local energy gap modulation. Notice that we did not solve the effective Hamiltonian of Eq.(27), but extracted the energy gap along the axis by considering the spectrum of the effective one-dimensional theory (Eq.7), obtained by dimensional reduction. Solving the equation for a general A without the dimensional reduction would be difficult even in the absence of mixing because the eigenfunctions of Hamiltonian $H_K = E$ should also satisfy [22] as

$$H_K^2 = (p - A^i)^2_0 + hB_i^3 = E^2; \quad (65)$$

where we have set $v_F = 1$ and $A^{\text{em}} = 0$. The spectrum of the first term on the right-hand side is known to be quite nontrivial even for simple vortex configurations [23]. Furthermore, it is already difficult to solve the one-dimensional Hamiltonian because of the local modulation mass term. The nature of the wave function should

be important for investigating the possibility of "energy gap engineering" which requires a multiple quantum dots prepared by a local modulation of the energy gap.

VII. CONCLUSION

We have examined the effects of surface deformation on the ground state of conducting electrons using the nearest-neighbor tight-binding Hamiltonian. Within a framework of the effective-mass theory, we clarified the relationship between local deformation of the lattice and the local energy gap along the axis in terms of the deformation-induced magnetic field. We formulated an effective theory describing the dynamics on

a general deformed surface, including topological defects that can cause a mixing of the two Fermi points. The theory is formally equivalent to the Weyl equation in U(1) Abelian and SU(2) non-Abelian deformation-induced gauge fields.

Acknowledgments

K.S. is supported by a fellowship of the 21st Century COE Program of the International Center of Research and Education for Materials of Tohoku University. R.S. acknowledges a Grant-in-Aid (No. 13440091) from the Ministry of Education, Japan.

[1] S. Iijima, *Nature* 354, 56 (1991).

[2] R. Saito, G. D. Dresselhaus, and M. S. Dresselhaus, *Physical Properties of Carbon Nanotubes*, Imperial College Press, London (1998).

[3] J.W. G. W. Wildeoer, L.C. Venema, A.G.R. Amesz, R.E. Smalley, and C. Dekker, *Nature* 391, 59 (1998); T.W. Odom, J. Huang, P. Kim, and C.M. Lieber, *Nature* 391, 62 (1998).

[4] J.C. Slonczewski and P.R. Weiss, *Phys. Rev.* 109, 272 (1958).

[5] C.L. Kane and E.J. Mele, *Phys. Rev. Lett.* 78, 1932 (1997).

[6] M. Ouyang, J. Huang, C.L. Cheung, and C.M. Lieber, *Science* 292, 27 (2001).

[7] A. Kleiner and S. Eggert, *Phys. Rev. B* 64, 113402 (2001); 63, 73408 (2001); L.F. Chibotaru, S.A. Bovin, and A. Ceulemans, *Phys. Rev. B* 66, 161401 (2002).

[8] T. Ando, T. Nakanishi, and R. Saito, *J. Phys. Soc. Jpn.* 67, 2857 (1998).

[9] J. Lee, H. Kim, S.-J. Kahng, G. Kim, Y.-W. Son, J. Ihm, H. Kato, Z.W. Wang, T. Okazaki, H. Shinohara, and Y. Kuk, *Nature* 415, 1005 (2002).

[10] J.M. Luttinger and W. Kohn, *Phys. Rev.* 97, 869 (1955).

[11] H. Suzuura and T. Ando, *Phys. Rev. B* 65, 235412 (2002).

[12] S. Tomonaga, *Prog. Theor. Phys.* 5, 544 (1950).

[13] R. Jackiw and C. Rebbi, *Phys. Rev. D* 13, 3398 (1976).

[14] C.H. Xu, C.Z. Wang, C.T. Chan, and K.M. Ho, *J. Phys.: Condens. Matter* 4, 6047 (1992); L.G. Gooch, A.J. Skinner, and D.G. Pettifor, *Europhys. Lett.* 9, 701 (1989).

[15] J. Jiang, R. Saito, A.G. Rueneis, G. Dresselhaus, and M. S. Dresselhaus, (unpublished).

[16] Y. Cho, S. Han, G. Kim, H. Lee, and J. Ihm, *Phys. Rev. Lett.* 90, 106402 (2003); see also D. Hombaker, S. Kahng, S. Misra, B. Smith, A. Johnson, E. Mele, D. Luzzi, and A. Yazdani, *Science* 295, 828 (2002).

[17] N.A. Vjet, H. Ajiki, and T. Ando, *J. Phys. Soc. Jpn.* 63, 3036 (1994).

[18] H. Ajiki and T. Ando, *J. Phys. Soc. Jpn.* 62, 2470 (1993), *Solid State Comm.* 102, 135 (1997); J. Kono, G.N. Ostojic, S. Zaric, M.S. Strano, V.C.M. Moore, J. Shaver, R.H. Hauge and R.E. Smalley, *App. Phys. A* 78, 1093 (2004).

[19] J. Gonzalez, F. Guinea, and M.A. Vozmediano, *Phys. Rev. Lett.* 69, 172 (1992), *Nucl. Phys. B* 406, 771 (1993); H. Matsumura and T. Ando, *J. Phys. Soc. Jpn.* 67, 3542 (1998), 70, 2657 (2001); P.E. Lamberton and V.H. Crespi, *Phys. Rev. Lett.* 85, 5190 (2000).

[20] K. Sasaki, Y. Kawazoe, and R. Saito, *Phys. Lett. A* 321, 369 (2004).

[21] H. Terrones and M. Terrones, *New Journal of Physics* 5, 126.1–126.37 (2003).

[22] R. Jackiw, *Phys. Rev. D* 29, 2375 (1984).

[23] Y. Aharonov and D. Bohm, *Phys. Rev.* 115, 485 (1959); R. Jackiw, *Ann. Phys.* 201, 83 (1990); Y. Nambu, *Nucl. Phys. B* 579, 590 (2000).